Real-time reception of NHS-OFDM signal with SPA-enhanced channel estimation for IMDD systems

Gang Chen (陈 港), Ming Chen (陈 明)*, Wen Chen (陈 雯), Lede Yin (尹乐得), Aitao Deng (邓爱桃), Yuxin Cai (蔡宇昕), and Dengqiao Wang (王邓桥)

School of Physics and Electronics, Hunan Normal University, Changsha 410081, China

* Corresponding author: *ming.chen@hunnu.edu.cn*

In this letter, we have experimentally verified a low-complexity subcarrier pairwise-averaging (SPA) enhanced channel estimation (CE) method for small-size FFT non-Hermitian symmetric orthogonal frequency-division multiplexing (NHS-OFDM) transceivers. Compared with intra-symbol frequency-averaging (ISFA), more than 20% look-up tables and 10% logic power consumption can be saved. The least-square (LS), ISFA and SPA CE methods are compared by offline and real-time digital signal processing (DSP) approaches. The results show that the receiver sensitivity of the SPA NHS-OFDM transmission system with 64/128-point FFT can be improved by more than 1 dB at the bit error rate of 3.8e-3, compared to the LS.

Keywords*:* NHS-OFDM; least-square; intra-symbol frequency-averaging; subcarrier pairwise-averaging
DOI: 10.3788/COL202220.050601

1. Introduction

Recently, with the development of high bandwidth services such as high-definition digital TV, video conference, Internet of things (IoT) and the fifth-generation (5G) mobile network, users' demand for access network bandwidth is becoming higher and higher [1,2]. To meet people's increasing demand for bandwidth, orthogonal frequency-division multiplexing (OFDM) technology is considered to be one of the key candidate technologies for short-reach application scenarios such as passive optical networks and optical interconnects in data centers since its high spectral efficiency (SE), strong resistance to fiber dispersion [3-6]. Compared with coherent optical OFDM (CO-OFDM) [7-8] with complex system structure, intensity-modulated direct-detection optical OFDM (IMDDO-OFDM) [9] has been widely studied because of its simple structure, low complexity and low cost. The real-valued OFDM signal is obtained when the input data of IFFT is constrained with Hermitian symmetry (HS). We call this type of OFDM as HS-OFDM. In another case, the output data of the IFFT are complex-valued ones since the HS constraint is not performed, which is defined as non-Hermitian symmetric OFDM (NHS-OFDM) in this work. In general, multiple data converters combined with analog up/down-conversion [10] or digital up/down-conversion [11] are required in the NHS-OFDM system. In [12], a low-complexity NHS-OFDM signal generation and reception method without up/down conversions was proposed. It generates 2*N* real-valued discrete OFDM signals by juxtaposing the *N* real and *N* imaginary parts of the *N*-point complex-valued IFFT outputs in the time domain. It indicates that under the same bandwidth granularity, NHS-OFDM can make full use of the FFT algorithm compared with HS-OFDM, to reduce the hardware implementation complexity. Besides, the same SE and peak to average power ratio (PAPR) performance as HS-OFDM can be achieved. In the following content, NHS-OFDM refers to the low-complexity NHS-OFDM proposed in [12], unless otherwise stated. Numerical simulation [13], offline [14] and real-time [15] demonstrations show that the NHS-OFDM has a similar bit error rate (BER) performance with the HS-OFDM.

The transmission performance depends on the accuracy of channel estimation (CE). Least square (LS) and least mean square error (MMSE) are the two most common CE methods [16,17]. However, MMSE needs autocorrelation statistical channel and statistical working noise power, which results in high calculation complexity and a big challenge in the process of hardware implementation. In contrast, the LS algorithm with low complexity has been widely used in real-time HS-OFDM systems [18, 19]. However, the LS method is sensitive to various noises and interferences. To obtain an accurate estimate, multiple training sequences (TS) are transmitted for each OFDM frame. When a long frame is transmitted with one or fewer TSs, the overhead can be ignored. However, in practical applications, if short frames transmission is dominant, and then the SE is significantly reduced. An intra-symbol frequency-domain averaging (ISFA)-enhanced CE method based on a single TS for CO-OFDM was presented in [20]. For the ISFA method, partial noises and interferences may be suppressed by performing the averaging operation over the channel estimate of several adjacent subcarriers. A large number of offline investigations [21] on the ISFA have been conducted and exhibited that the CE method is robust to various transmission impairments in optical OFDM systems with large FFT sizes. However, large-size fully-parallel FFT algorithms for high-speed optical communications consume lots of chip resources in the hardware implementation process. In [22], the FFT module of a partially-parallel HS-OFDM transceiver accounts for more than 40% of the total logic resources. Therefore, a small-size FFT-based NHS-OFDM may be a better choice from the perspective of hardware implementation. However, subcarrier (SC) spacing is relatively large and the correlation of channel response on adjacent subcarriers may become worse in the optical OFDM system with small-size FFT algorithms. In this case, the ISFA method may not work effectively. In our previous work [21], we proposed and investigated a subcarrier pairwise-averaging (SPA) method to enhance the accuracy of CE for the NHS-OFDM system via offline experiments.

In this letter, the LS/ISFA/SPA-based real-time NHS-OFDM transceivers are designed and implemented. The on-chip resources and power consumption of SPA and ISFA methods are analyzed. The bit error rate (BER) performance is measured by offline and real-time DSP approaches in an IMDD NHS-OFDM system with 64/128-point FFT functions. The rest parts of this paper are organized as follows. Section 2 introduces the basic

principle of LS, ISFA and SPA methods in NHS-OFDM systems. Section 3 describes the experimental setup of the real-time NHS-OFDM transmission system. The hardware resources and logic power consumption of SPA and ISFA methods are compared, and the BER performance is analyzed under both offline and real-time measurements in Section 4. The conclusion is drawn in Section 5.

2. Operation Principle

In the NHS-OFDM transmitter, the pseudo-random binary sequence (PRBS) is first mapped into QAM symbols, and after performing the IFFT and adding cyclic prefix (CP) and TS. They are sent to the complex-to-real conversion (C2R) module, which juxtaposes the real and imaginary parts of the N-point complex-valued OFDM signal to generate $2N$ point real-valued signal. Fig. 1 shows the block diagram of the C2R operation and time-domain NHS-OFDM frame structure.

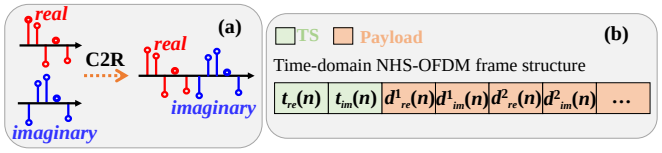

Fig. 1. Block diagram of (a) C2R operation and (b) NHS-OFDM time-domain frame structure.

In the NHS-OFDM receiver, the real and imaginary parts of the received time-domain discrete signal can be expressed as

$$\hat{t}_{re}(n) = t_{re}(n) \otimes h(n) + w_{re}(n) \tag{1}$$

$$\hat{t}_{im}(n) = t_{im}(n) \otimes h(n) + w_{im}(n) \tag{2}$$

where $h(n)$ represents impulse response and $t_{re}(n)/t_{im}(n)$ are real/imaginary parts of the local TS $t(n)$. And $w_{re}(n)$ and $w_{im}(n)$ are additive noises. The convolution operation is denoted by $\otimes$.

Once the timing synchronization is done, the real-to-complex conversion (R2C) module converts the $2N$-point real-valued TS into N-point complex-valued ones

$$\hat{t}(n) = \hat{t}_{re}(n) + j\hat{t}_{im}(n) \tag{3}$$

After CP removal, the frequency-domain data on the k-th SC of the received TS after FFT operation can be written by

$$\begin{aligned} \hat{T}(k) &= FFT\{\hat{t}(n)\} \\ &= FFT\{\hat{t}_{re}(n)\} + jFFT\{\hat{t}_{im}(n)\} \\ &= \frac{1}{2}\left[T(k) + T^*(-k)\right] \cdot H(k) + W_{re}(k) \\ &\quad + j\left(\frac{1}{2j}\left[T(k) - T^*(-k)\right] \cdot H(k) + W_{im}(k)\right) \\ &= T(k)H(k) + W_{re}(k) + jW_{im}(k) \end{aligned} \tag{4}$$

where $H(k)$, $T(k)$, $W_{re}(k)$ and $W_{im}(k)$ are frequency-domain forms of $h(n)$, $t(n)$, $w_{re}(n)$ and $w_{im}(n)$, respectively. Channel estimation can be realized with the LS method. The estimated channel response on the k-th data-carrying SC can be expressed as

$$\hat{H}_{LS}(k) = \frac{\hat{T}(k)}{T(k)} = H(k) + \frac{W_{re}(k) + jW_{im}(k)}{T(k)} \tag{5}$$

where the data-carrying SC index k ranges from $-k_{max}$ to $-k_{min}$ and k_{min} to k_{max} since there is not HS constraint. And other SCs are filled with zeros. Since $\hat{t}_{re}(n)$ and $\hat{t}_{im}(n)$ are real-valued signals, we can get the relationship of $H(k) = H^*(-k)$, $W_{re}(k) = W_{re}^*(-k)$ and $W_{im}(k) = W_{im}^*(-k)$. Therefore, $\hat{H}_{LS}(-k)$ can be expressed as

$$\hat{H}_{LS}(-k) = H^*(k) + \frac{W_{re}^*(k) + jW_{im}^*(k)}{T(-k)} \tag{6}$$

However, the single-TS-aided LS method is sensitive to various noises and interferences introduced by optical and electrical devices. To improve the accuracy of CE, the ISFA-enhanced CE method with high SE can be employed for the NHS-OFDM. The ISFA-enhanced CE based on LS can be defined as

$$\hat{H}_{ISFA}(k) = \begin{cases} \dfrac{1}{A-B+1}\displaystyle\sum_{k'=B}^{A} \hat{H}_{LS}(k'), k \in [-k_{max}, -k_{min}] \\ \dfrac{1}{C-D+1}\displaystyle\sum_{k'=D}^{C} \hat{H}_{LS}(k'), k \in [k_{min}, k_{max}] \\ A = min(-k_{min}, k+m) \\ B = max(-k_{max}, k-m) \\ C = min(k_{max}, k+m) \\ D = max(k_{min}, k-m) \end{cases} \tag{7}$$

The tap number of the ISFA is $2m+1$. When small size FFTs with large SC spacing are considered, this CE method may not work effectively since the channel response difference on adjacent SCs increases. A simple SPA-based CE method [21] is proposed to enhance the accuracy of CE in NHS-OFDM. The estimated channel response by the SPA is given by

$$\hat{H}_{SPA}(k) = \hat{H}_{SPA}^*(-k) = \frac{\hat{H}_{LS}(k) + \hat{H}_{LS}^*(-k)}{2} \tag{8}$$

In this work, $T(k)$ takes randomly from $\{\pm 1\}$. According to Eq. (5) and (6), $\hat{H}_{SPA}(k)$ can be further reduced to

$$\hat{H}_{SPA}(k) = \begin{cases} H(k) \pm W_{re}(k), & T_{TS}(k) = T_{TS}(-k) \\ H(k) \pm jW_{im}(k), & T_{TS}(k) = -T_{TS}(-k) \end{cases} \tag{9}$$

As we can see from Eq. (9), by using the SPA method, the accuracy of channel estimation can be improved by suppressing additive noises. For each data-carrying SC, only two real-valued addition and bitwise shift operations are required for the hardware implementation of the SPA method. In contrast, the ISFA method needs at least four real-valued addition and division (or more complicated bit shift) operations.

3. Experimental Setup

To fully verify the performance of the SPA method in the NHS-OFDM system with small-size FFTs, the FPGA-based real-time NHS-OFDM transmission system with IMDD is established and shown in Fig. 2. In the optical NHS-OFDM transmitter, a PRBS with a length of 2^{15}-1 is generated offline and stored in the ROM of the FPGA. The control unit (CU) pushes the PBRS sequence into the QAM mapping module by controlling the address of the PRBS ROM. The mapped symbols are used to modulate 50 (100) data-carrying SCs with indices from -25 to 25 (-50 to 50) excluding zero. The direct current (DC) SC and 13 (27) high-frequency SCs are filled with zeros for the NHS-OFDM with 64(128)-point IFFT functions. The eight complex-valued

frequency-domain data in parallel are sent to the IFFT function to obtain the complex-valued time-domain data. A CP with a length of 8 is added in front of the IFFT output to resist inter-symbol interference (ISI) [24]. To reduce the PAPR of the NHS-OFDM signal, digital clipping with a clipping ratio of 12 dB is performed. Afterward, the clipped data is scaled to 14-bit data to adapt to the resolution of the DAC (ADI, AD9739A). After that, the 8 complex-valued data in parallel are converted into 16 real-valued ones in parallel by using two FIFOs. The adopted C2R method is similar to our previous work [15]. To achieve symbol synchronization, CE and channel equalization, the real-valued TS with a length of 144 (272) and 14-bit resolution is offline generated and stored in FPGA registers. Under the control of the CU module, single TS and multiple data-carrying NHS-OFDM symbols are sent to the DAC interface module, which mainly completes the parallel-to-serial conversion, FPGA working clock (156.25 MHz) generation and signed data to unsigned data conversion. Subsequently, the serialized data is sent to the 2.5 GSa/s DAC chip through the low-voltage differential signaling (LVDS) interface. The differential baseband NHS-OFDM signal from DAC is converted into a single-ended signal through the first balun. A low-pass filter (LPF) with a 3-dB bandwidth of 1 GHz is used to suppress the DAC high-frequency image. The filtered signal is attenuated by a 3-dB fixed attenuator (ATT) to reduce nonlinear distortion induced by the electrical amplifier (EA, ZX60-14012L-S+), amplified and added an 80mA bias current to drive a C-band 10 GHz directly-modulated laser (DML, NLK1551SSC). The optical signal is coupled into 20 km SSMF (ITU-T G.652) for transmission.

In the real-time optical NHS-OFDM receiver, a variable optical attenuator (VOA) is placed in front of the optical coupler (OC) with a split ratio of 10:90 to change the received optical power (ROP), and indirectly measure the ROP by a power meter (PM). The signal with 90% power from the OC is directly detected by a PIN photodiode (PD). The recovered signal is amplified by a 4.5 GHz EA, converted into the differential signal via the second balun, and sampled by a 2.5 GSa/s time-interleaved analog-to-digital converter (ADC). The captured samples are sent to Xilinx Virtex-7 FPGA (XC7VX485T-2FFG1761) evaluation board VC707 through the LVDS interface. A common clock source is employed to avoid the sampling clock frequency offset (SFO) between the receiver and the transmitter. The received samples from the ADC chip are performed serial-to-parallel conversion and unsigned data converted to signed data through the ADC interface module. And then the offset mismatch compensation (OMC) caused by TI-ADC is conducted [25]. After completing the low-complexity symbol synchronization based on TS, the real-to-complex conversion (R2C) module is realized. Next procedures include the CP removal, 64/128-point FFT, CE and channel equalization and QAM De-mapping. The error bit count is sent to a personal computer (PC) through the Xilinx ChipScope Pro tool for real-time error measurement. In addition, the OFDM samples captured by the ADC are also saved and uploaded to PC for comparison and analysis by using offline DSP approaches.

Insets 2(b) and 2(c) are the baseband NHS-OFDM transceiver hardware platform. The register-transfer level (RTL) schematics of the real-time NHS-OFDM transceiver are given in Figs. 2(d) and 2(e). In addition, some key parameters for the experiment are shown in Table 1.

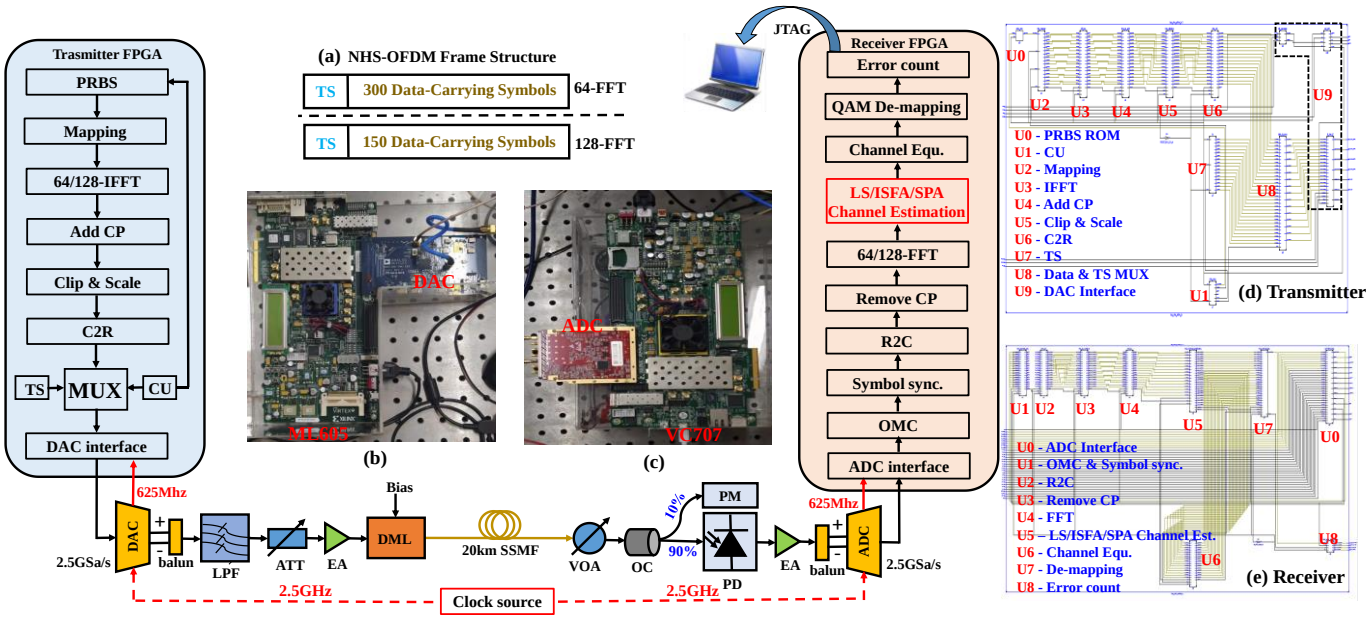

Fig. 2. Experimental setup of the real-time NHS-OFDM transmission system with IMDD. Inset (a) is OFDM frame structure, (b)-(c) are the baseband transceivers hardware platforms, and (d)-(e) are the RTL schematics of the real-time NHS-OFDM transceiver.

Table 1. Some key parameters used in the experiment

Item	Parameter	Value		Unit
		NHS-OFDM		
OFDM frame	Modulation format	16QAM		-
	IFFT/FFT	64	128	points
	Data SCs	50	100	-
	CP length	8		points
	TS symbols per frame	1		-
	Data-carrying OFDM symbols	300	150	-
	Digital clipping ratio	12		dB
	Net signal bit rate	3.46	3.65	Gb/s
	Spectral efficiency	3.54	3.74	bits/s/Hz
	OFDM Frame duration	17.34	16.43	us
DAC & ADC	Sampling rate	2.5		GS/s
	Resolution	14/10		bits
LPF	Bandwidth	~1		GHz
	Depth	30		dB
EA1&2	Bandwidth	12 (4.5)		GHz
DML	Operation wavelength	1556.3		nm
	Output power	2.3		dBm
SSMF	Length	20		km
	Attenuation	0.18		dB/km
	Dispersion	17		ps/nm/km
PIN	Bandwidth	10		GHz
	Coupling mode	AC		-

4. Results and Discussion

4.1 Offline Investigations

To identify the optimal taps for the ISFA algorithm in the NHS-OFDM receiver with small-size FFT functions, we first offline investigate the amplitude response and error vector magnitude (EVM) performance. In the offline experiments, each frame contains one TS and 800/400/200 data symbols in the NHS-OFDM system with 64/128/256-point FFT functions. The number of data-carrying SCs is 50/100/200 and the CP length is 1/8 FFT size. The offline generated discrete frame signal is stored in FPGA ROMs and sent to the DAC chip periodically for data conversion. In the offline receiver, the samples captured by the ADC are directly uploaded to the PC for offline signal processing. Note that the offline DSP approaches are the same as the real-time ones.

At the ROP of -6 dBm, the normalized amplitude responses (AR) with LS/ISFA/SPA methods as a function of data-carrying SC index for 64/128/256-point FFTs are analyzed and shown in Figs. 3(a)-(c). It can be seen that the power fading on high-frequency SCs exceeds 7 dB. This is mainly due to the imperfect frequency response of DAC, EA and LPF. In our experiment, 20km SSMF is used for transmission, and the bandwidth of the OFDM signal is ~1GHz. So the power fading induced by chromatic dispersion is negligible. In addition, the amplitude fluctuation on some adjacent SCs exceeds 1.8dB. The corresponding EVM performance under different ROPs is presented in Figs. 3(d)-(f). The relevant results indicate the SPA can provide better EVM performance than the conventional LS and ISFA with taps of 3, 5 and 7 for 64/128-point FFTs-enabled NHS-OFDM systems. This achievement benefits from the accurate channel estimate by using SPA. Since the channel response on some adjacent SCs may fluctuate greatly, the ISFA with more averaging taps (the number of adjacent SCs) makes inaccurate channel estimate; therefore, ISFA cannot work effectively in small-size FFTs-enabled NHS-OFDM systems. However, we also observe that the ISFA with 3 taps can achieve a similar EVM performance with SPA when the 256-point FFT is used. In this case, large-size FFTs can provide smaller SC spacing and then makes the channel estimation more accurate even for the LS method. At the same time, a smaller difference in channel response on adjacent SCs can be achieved. After averaging the operation of SPA and ISFA, the accuracy of CE can be further improved. Therefore, we can see clearly the increased EVM performance as the FFT size increases. However, large-size FFT will increase hardware implementation complexity and power consumption.

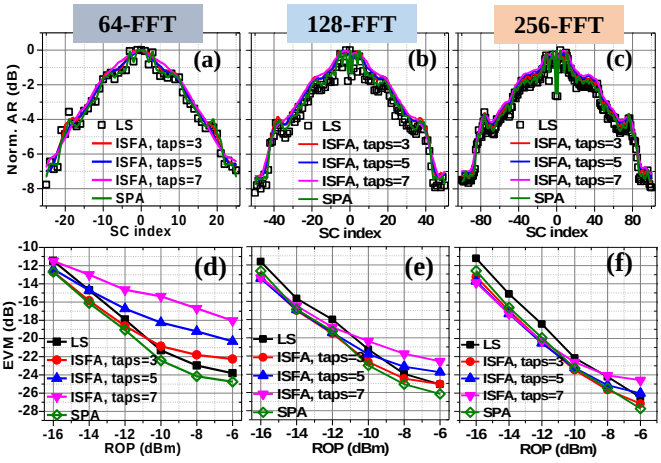

Fig. 3. (a)-(c) The normalized amplitude response and (d)-(e) the EVM performance for 64/128/256-point FFTs.

The recovered constellation diagrams and corresponding EVM values with LS/ISFA/SPA methods are given in Fig. 4. Compared with the LS and ISFA methods, the SPA method can provide 1/1.1/1.2dB and 2.5/1.1/0.5dB EVM performance improvements, respectively, in 64/128/256-point FFTs-based NHS-OFDM transmission systems. When 64/128-point FFTs are employed, the constellations recovered by the ISFA method have obvious divergence, and its EVM performance is degraded by 1.5 dB, compared to the LS method. In the 256-point FFT case, similar EVM performance is observed for SPA and ISFA, since larger-size FFT make a small difference in channel response on adjacent SCs and realize accurate channel estimates [26].

Hence, we only investigate the small-size 64/128-point FFTs in the FPGA-based NHS-OFDM transceiver and use the ISFA method with the optimal ISFA taps of 3 in the following discussion.

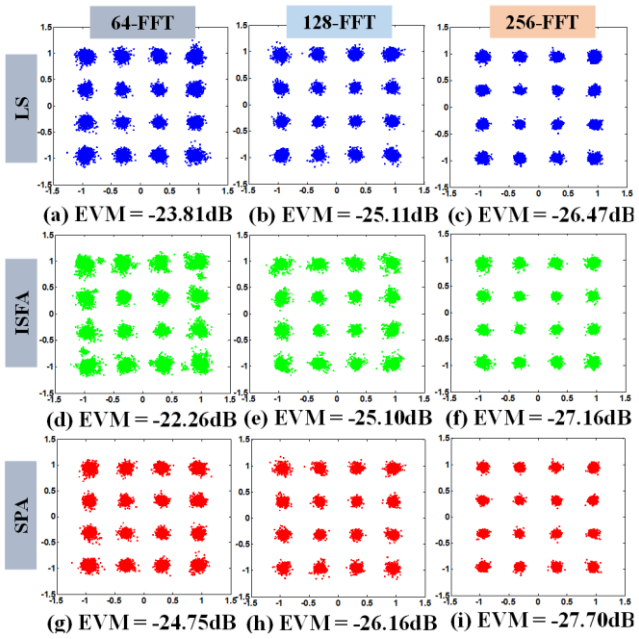

Fig. 4. Recovered constellation diagrams: (a)-(c) LS, (d)-(f) ISFA and (g)-(i) SPA for different FFT sizes.

4.2 Real-time BER Performance

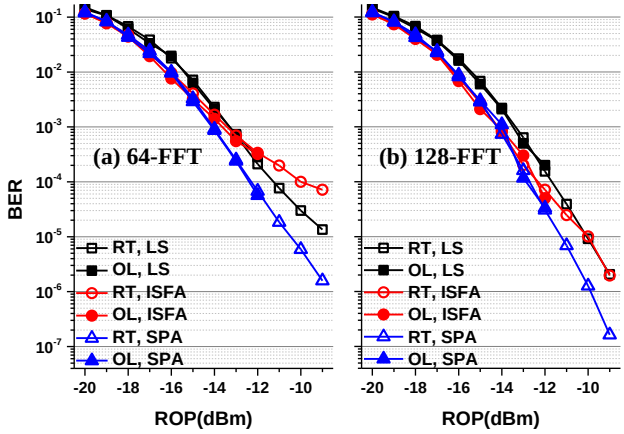

Fig. 5. Real-time and offline measured BER performance versus ROP: (a) 64-point and (b) 128-point FFTs.

The BER performance with the three CE methods after 20 km SSMF transmission over different ROPs is measured by real-time and offline DSP approaches. The relevant results for 64- and 128-point FFTs are presented in Fig. 5(a) and 5(b), respectively. It indicates that the real-time BER performance is the same as the offline one. Note that the offline measured BER values of one frame are zero and not shown in Fig. 5 when the ROP is greater than 12 dBm. In our real-time measurements, we count errors of 61,440,000 bits carried by consecutive 1,024 frames. In addition, at the BER of 3.8e-3, the receiver sensitivity with 64-point FFT and the SPA can be improved by 1.1 dB and 0.5 dB compared with LS and ISFA methods, respectively. At the BER of 1e-4, about 1 and 2 dB improvements in receiver sensitivity can be achieved with the SPA method in the 128-point FFT case, compared to ISFA and LS methods, respectively. These facts are mainly attributed to the accurate channel estimation provided by the SPA method. It should be noted that the ISFA/SPA can be extended to high-speed optical NHS-OFDM and work effectively [21].

4.3 Hardware complexity and power consumption

The on-chip resource usages for the SPA and ISFA CE modules implemented in real-time NHS-OFDM receivers with 64/128/256-point FFTs are analyzed and listed in Table 2. The SPA method uses a similar number of registers compared to ISFA. However, the SPA saves 817/1190/2067 look-up tables (LUTs) for the receivers with 64/128/256-point FFTs. In fact, the SPA method can be regarded as a special ISFA with two taps; therefore, it can save 100/200/400 real-value adders in each data symbol compared with the ISFA, and LUTs can be saved by 28.4%/21.9%/19.5%. Note that the hardware implementation of SPA and ISFA modules does not use any multipliers or dividers since these operations are equivalently implemented with addition and bitwise shift operations. In addition, we also use XPower Analyzer tool to estimate the power consumption. About 19%/14%/14% on-chip power consumption can be saved by using the SPA method, compared to the ISFA.

Table 2. The device utilization of the SPA/ISFA sub-module in NHS-OFDM with 64/128/256-point FFT functions.

FFT size	CE methods	Registers	LUTs
64	ISFA	2256	2877
	SPA	2160	2060
128	ISFA	4048	5428
	SPA	4080	4238
256	ISFA	7632	10612
	SPA	7630	8545

5. Conclusion

In this work, we experimentally verified a low-complexity SPA-enhanced CE method in a small-size FFT-enabled real-time NHS-OFDM system with IMDD. The experimental results showed that the receiver sensitivity can be improved by more than 1 dB by employing the SPA CE method at the BER of 3.8e-3, compared to the conventional LS method. Moreover, the SPA outperforms the ISFA in 64/128-point FFT cases regarding EVM/BER performance, hardware implementation complexity and power consumption.

Acknowledgments

This work was supported in part by the National Natural Science Foundation of China under Grant 61805079, in part by the Hunan Provincial Natural Science Foundation of China under Grant 2020JJ4433, and in part by the Hunan Province College Students Research Learning and Innovative Experiment Project, China under Grant S202010542058.

References

1. B. J. C. Schmidt, A. J. Lowery, and J. Armstrong, "Experimental demonstrations of electronic dispersion compensation for long-haul transmission using direct detection optical OFDM," J. Lightwave Technol. 26, 196 (2008).
2. Armstrong, Jean. "OFDM for optical communications." J. Lightwave technol. 27, 189 (2009).
3. J. Xu, M. Jiang, and Y. Chen. "OFDM-based visible light communication with rotated polarity modulation aided complex color shift keying," Chin. Opt. Lett. 17, 100602 (2019).
4. Y. Xiao, Z. Wang, J. Cao, R. Deng, Y. Liu, J. He, and L. Chen, "Time-Frequency Domain Encryption With SLM Scheme for Physical-Layer Security in an OFDM-PON System," J. Opt. Commun. Netw. 10, 46 (2018).

5. L. Chen, J. Zhou, Y. Qiao, Z. Huang, and Y. Ji, "Novel modulation scheme based on asymmetrically clipped optical orthogonal frequency division multiplexing for next-generation passive optical networks," J. Opt. Commun. Netw. 5, 881 (2013).
6. M. Chen, L. Wang, D. Xi, L. Zhang, H. Zhou, and Q. Chen, "Comparison of Different Precoding Techniques for Unbalanced Impairments Compensation in Short-Reach DMT Transmission Systems," J. Lightwave Technol. 38, 6202 (2020).
7. W. Shieh, and C. Athaudage. "Coherent optical orthogonal frequency division multiplexing," Electronics Letters 42, 587 (2006).
8. Y. Jiang, X. Yi, S. Hu, X. T. Huang, W. Tang, W. Zhou, X. N. Huang, J. Zhang, and K. Qiu. "Polarization de-multiplexing using a modified Kalman filter in CO-OFDM transmissions," Chin. Opt. Lett. 17, 030603 (2019).
9. D. Qian, J. Hu, J. Yu, J. Yu, P. N. Ji, L. Xu, T. Wang, M. Cvijetic, and T. Kusano, "Experimental demonstration of a novel OFDM-A based 10Gb/s PON architecture," Proc. ECOC (2007).
10. S. L. Jansen, I. Morita, T. C. W. Schenk, and H. Tanaka, "121.9-Gb/s PDM-OFDM transmission with 2-b/s/Hz spectral efficiency over 1000 km of SSMF," J. Lightw. Technol., 27, 177 (2009).
11. L. Nadal, J. M. Fabrega, J. Vilchez, and M. Svaluto Moreolo, "Experimental Analysis of 8-QAM Constellations for Adaptive Optical OFDM Systems," IEEE Photon. Technol. Lett. 28, 445 (2016).
12. F. Barrami, Y. L. Guennec, E. Novakov, J. M. Duchamp, and P. Busson, "A novel FFT/IFFT size efficient technique to generate real time optical OFDM signals compatible with IM/DD systems," in: Proc. Eur. Microw. Conf., 1247 (2013).
13. M. F. Sanya, L. Djogbe, A. Vianou, and C. Aupetit-Berthelemot, "DC biased optical OFDM for IM/DD passive optical network systems," J. Opt. Commun. Netw. 7, 205 (2015).
14. M. Chen, X. Xiao, Z. R. Huang, J. Yu, F. Li, Q. Chen, and L. Chen, "Experimental Demonstration of an IFFT/FFT Size Efficient DFT-Spread OFDM for Short Reach Optical Transmission Systems," J. Lightwave. Technol. 34, 2100 (2015).
15. G. Chen, M. Chen, W. Chen, L. Yin, L. Zhang, D. Xi, H. Long, L. Wang, S. Qian, and Q. Chen, "Hardware-efficient generation and reception of NHS-OFDM signal for direct-detection PON," Opt. Commun. 508, 127721 (2022).
16. Y. S. Hussein, M. Y. Alias, and A. A. Abdulkafi, "On performance analysis of LS and MMSE for CE in VLC systems," 2016 IEEE 12th International Colloquium on Signal Processing & Its Applications (CSPA). IEEE, 204 (2016).
17. X. Chen, and M. Jiang, "Adaptive statistical Bayesian MMSE CE for visible light communication," IEEE transactions on signal processing, 65, 1287 (2016).
18. M. Chen, P. Zou, L. Zhang, and N. Chi, "Demonstration of a 2.34 Gbit/s real-time single silicon-substrate blue LED-based underwater VLC system," IEEE Photon. J. 12, 1 (2020).
19. R. Deng, J. He, M. Chen, and Y. Zhou, "Experimental demonstration of a real-time gigabit OFDM-VLC system with a cost-efficient precoding scheme," Opt. Commun. 423, 69 (2018).
20. X. Liu, and F. Buchali, "Intra-symbol frequency-domain averaging based CE for coherent optical OFDM," Opt. Express 16, 21944 (2008).
21. F. Li, J. Yu, Y. Fang, Z. Dong, X. Li, and L. Chen, "Demonstration of DFT-spread 256 QAM-OFDM signal transmission with costeffective directly modulated laser," Opt. Express 22, 8742 (2014).
22. J. S. Bruno, V. Almenar, J. Valls, and J. L. Corral, "Real-time 20.37 Gb/s optical OFDM receiver for PON IM/DD systems," Opt. Express 26, 18817 (2018).
23. L. Yin, W. Chen, M. Chen, S. Qian, G. Chen, J. Zuo, and Q. Cheng, "Demodulation of NHS-OFDM Signal with Real-valued FFT and Enhanced Channel Estimation," Asia Communications and Photonics Conference T4A.75 (2021).
24. R. Deng, J. He, M. Chen, and L. Chen. "SFO compensation by pilot-aided CE for real-time DDO-OFDM system," Opt. Commun. 355,172 (2015).
25. M. Chen, G. Liu, L. Zhang, H. Zhou, and Q. Chen, "Online digital offset mismatch compensation for high-speed time-interleaved ADC in real-time optical OFDM receiver," Opt. Express 27, 16650 (2019).
26. F. Li, X. Li, L. Chen, Y. Xia, C. Ge, and Y. Chen, "High level QAM OFDM system using DML for low-cost short reach optical communications," IEEE Photon. Technol. Lett. 26, 941 (2014).